Applied Catalysis B: Environmental 92 (2009) 217–224

Contents lists available at ScienceDirect

Applied Catalysis B: Environmental

journal homepage: www.elsevier.com/locate/apcatb

In situ characterizations of Pd/Al_2O_3 and $Pd/CeO_2/Al_2O_3$ catalysts for oxidative steam reforming of propane

Wagner L.S. Faria, Carlos A.C. Perez, Deborah V. César, Lídia C. Dieguez, Martin Schmal *

NUCAT/PEQ/COPPE, Federal University of Rio de Janeiro, C.P. 68502, 21945-970 Rio de Janeiro, Brazil

ARTICLE INFO

Article history:
Received 12 January 2009
Received in revised form 27 June 2009
Accepted 2 July 2009
Available online 10 July 2009

Keywords:
DRIFTS
XRD *in situ*
Propane
Ceria
Palladium

ABSTRACT

Catalytic activity results of oxidative steam reforming of propane studied on Pd catalysts are here explained on the basis of different characterization analyses under reaction conditions. XRD *in situ* was applied to investigate nanostructure features by means of a Rietveld refinement giving additional information about ceria lattice parameter along the reaction. The refinement was applied in all pretreatment steps, after reduction and after reaction. A good correlation was obtained in all conditions. The mean crystallite sizes were calculated for CeO_2, Pd^0 and PdO at the higher intensity planes. Results of crystallite sizes after reaction during 1, 3, 8 and 20 h were determined. One can conclude that CeO_2 enhances and maintains the dispersion of Pd on bulk catalyst and prevents Pd from severe aggregation along the reaction because no sintering was detected even after 20 h of reaction. The changes in lattice cell parameter determined by Rietveld refinement suggested high oxygen mobility inside the fluoritic structure, facilitating formation of CeO_{2-x} species. DRIFTS were carried out under static and dynamic measurements and compared with TPD of propane in the presence of oxygen. These results showed formation of surface intermediate species (formates/carbonates) and CH_z species on surface during the oxidative steam reforming of propane that allows proposing a surface reaction mechanism.

1. Introduction

Hydrogen can be produced from different processes for use in fuel cells [1,2] for energy generation [3]. The autothermal reforming or oxidative steam reforming has the main advantage that the initial oxidation reaction is extremely exothermic, generating heat for the subsequent endothermic reforming reactions [4,5]. Among various hydrocarbons, propane is drawing attention in hydrogen production studies primarily because it is a constituent of LPG [6,7]. Propane is produced in relative high amounts from natural gas and oil crude refining. For pressures of approximately 9 bar, it is in liquid state and can be easily stored and distributed [8,9].

Palladium is very active for hydrocarbons and CH_4 oxidation [10]. On the other hand, cerium oxide (CeO_2) has been widely used as promoter due to its high oxygen storage capacity (OSC) [11], acting as thermal stabilizer of the support [12,13], allowing better dispersion of the metal [14] and preventing coke formation [15,16].

Information about propane oxidative steam reforming (OSR) *in situ* studies is relatively scarce in the literature and different reaction conditions used in some papers prevent an adequate comparison between results. Besides, many studies refer to methane, with little emphasis to propane.

In a previous paper [17], we studied the propane autothermal reforming on supported CeO_2/Al_2O_3 based Pd catalysts, prepared with different Pd precursors. The reaction was carried out under different feedstock conditions and the catalytic activity was evaluated by temperature programmed surface reaction (TPSR). The Pd effects precursor in activity was studied as well to maximize the H_2/CO ratio. The Pd acetylacetonate precursor catalyst showed the most active, the start temperature of reforming was 100 K less than Pd chlorine precursor catalyst. We obtained high hydrogen production by OSR or autothermal reforming of propane on $Pd/CeO_2/Al_2O_3$ catalysts, under sub-stoichiometric conditions ($O_2/C_3H_8 < 5$) in the presence and absence of water. There were two distinct regions in the composition profile, when hydrogen is formed by steam reforming (after complete oxygen consumption) with the residual propane and water produced in the primary total oxidation. At higher ratios ($O_2/C_3H_8 > 5$), only propane total oxidation generating CO_2 and H_2O was observed.

According to thermodynamic calculations, the optimum O_2/C_3H_8 ratio for hydrogen production is between 1.5 and 2.5. In this interval, the results showed for $R = 2.5$ the highest value for H_2/CO. Additionally, the $Pd/CeO_2/Al_2O_3$ presented higher hydrogen

* Corresponding author. Tel.: +55 21 2562 8352; fax: +55 21 2562 8300.
E-mail address: schmal@peq.coppe.ufrj.br (M. Schmal).

0926-3373/$ – see front matter © 2009 Elsevier B.V. All rights reserved.
doi:10.1016/j.apcatb.2009.07.001

production compared to Pd/Al_2O_3. The presence of CeO_2 increased the H_2/CO ratio in outlet gas and influenced positively to a large extent the high activity due to the water gas shift (WGS) reaction. The catalysts were stable for 50 h with small deactivation only in the first hours of reaction [17].

In this study, the *in situ* characterizations aiming to study the interaction of gaseous species with the surface and the formation and stability of the resulting surface species under reaction conditions will be investigated for OSR of propane over $Pd/CeO_2/Al_2O_3$ catalysts. In addition, palladium crystallites in the presence of CeO_2 were evaluated along the reaction by XRD.

2. Experimental

The CeO_2/Al_2O_3 system was prepared by grafting a cerium acetylacetonate precursor ($Ce(acac)_3$) (Aldrich Corp.) over alumina (AL-3916P-Engelhard Corp., 208 m^2/g and 0.47 cm^3/g) surface hydroxyl groups, as described elsewhere [16]. The grafting reaction had the objective of increasing the preparation efficiency in order to obtain well-dispersed ceria particles. The CeO_2 content was 18%, which is very close to the theoretical monolayer. After grafting, the sample was filtered and washed with toluene (Vetec, 99% P.A.) and distilled water, followed by drying in an oven at 393 K for 18 h and calcination under O_2 flow at 673 K for 4 h, using a heating rate of 1 K min^{-1}. The global process of preparation of the CeO_2/Al_2O_3 support (grafting, filtration, drying and calcination) was carried out in six stages due to the low solubility of $Ce(acac)_3$ in toluene.

The $Pd/CeO_2/Al_2O_3$ (1% Pd) catalyst was prepared using wet impregnation method. Toluene was used to dissolve $Pd(acac)_2$ and the system was then filtered. Finally, the sample was dried at 393 K for 18 h and calcined in an aerated muffle at 773 K for 4 h. Additionally, Pd/Al_2O_3 (1% Pd) was prepared using the same methodology and Pd precursor salt. The Pd content was 0.94(±0.03)%. H_2 and CO uptakes were obtained by chemisorption presenting results of 2.39 and 4.57 $\mu mol/mg_{Pd}$ for Pd/Al_2O_3 and 2.36 and 4.61 $\mu mol/mg_{Pd}$ for $Pd/CeO_2/Al_2O_3$, respectively, which are very close. Noteworthy is that the ratios of CO/H_2 are very similar equal to 1.93(±0.03) for both samples.

The dispersions measured by chemisorption were checked by FTIR CO adsorption, as reported previously [16,18], assuming total reduction of palladium. The calculated dispersions agreed very well.

Diffuse Reflectance Spectra (DRS) experiments were performed to determine the oxidation state of Pd and ceria after aging for 48 h under different reaction conditions ($R = 2.5$ and $S = 6$) and compared to fresh catalyst. The feed reaction consisted of 0.5% C_3H_8 and 0.5R% O_2 diluted in He, where R is defined as the O_2/C_3H_8 molar ratio. Experiments containing water in the inlet composition were denoted by S, where S represents the H_2O/C_3H_8 molar ratio. DRS were performed in an UV–vis range spectrometer Varian, model Cary 5, equipped with a diffuse reflectance accessory 'Harrick' with 'Mantis Prayning' geometry. The DRS analysis was done at room temperature in the range between 200 and 800 nm wavelength. The samples were aged or calcined (fresh samples) *ex situ* and introduced under inert gas in the chamber immediately after reaction, diluted in γ-Al_2O_3 at 1:5 ratio to avoid reflections. γ-Al_2O_3 was used as reference. The DRS spectra were presented using the Schulz–Kubelka–Munk's equation ($f(R)$).

Powder *in situ* X-ray diffractions (XRD) were carried out in a Rigaku DMAX 2500 PC diffractometer equipped with a pretreatment chamber able to reach high temperatures. The step-scans were taken over the range of 2θ from 10° to 80° in step of 0.02° and the intensity data for each one were collected for 10 s using Cu Kα radiation (λ = 1.5488 Å). The crystallite sizes (D_{XRD}) for ceria and palladium were determined with the Scherrer equation, using the values of the full-width at half-maximum (FWHM) from CeO_2, PdO and Pd peaks at $2\theta = 28.5°$, 33.9° and 40°, respectively. A peak broadening due to the instrumental broadening was taken into account using large CeO_2 particles ($d_{CeO_2} > 5$ mm; Sigma–Aldrich). All diffractograms were collected at 773 K, except for the fresh sample.

The samples were pretreated passing a flow of 5% O_2/He at 673 K for 60 min to eliminate carbonated species, probably formed on ceria [19], and followed by flowing He at 773 K for 90 min. These samples were reduced with pure H_2 at 773 K for 60 min and finally, degassed by flowing He at 773 K for 30 min. The oxidation stage was suppressed for catalysts supported only on γ-Al_2O_3. The diffractograms were collected after each pretreatment step and along the reaction (molar ratio O_2/C_3H_8 (R) = 2.5). According to our previous paper [17], this ratio provided high hydrogen condition among conditions applied. On this molar ratio (O_2/C_3H_8), H_2 is formed by steam reforming with the residual propane and water produced in the primary oxidation.

Crystalline structures were refined with the Rietveld technique by using FULLPROF® 98 code. The Rietveld refinement provided not only the concentration and average crystallite size of each phase present in the sample but also the lattice parameter and lattice defect information in the crystalline structures [20]. The lattice defects were determined by comparing the cation occupancy number with that present in the perfect ideal ceria. Besides, Rietveld method allows differentiating overlapping peaks in the diffraction pattern.

Diffuse Reflectance Infrared Fourier Transform Spectroscopy (DRIFTS) analyses have been carried in a Nicolet spectrometer (Nexus 470 model) with a MCT detector and equipped with a diffuse reflectance assembly (Spectra-Tech) chamber for high temperature treatment and ZnSe window. The samples, without dilution and packing, were pretreated *in situ* (as described earlier). After pretreatment, the inlet gas (R = 2.5) was introduced in the chamber. All spectra were obtained after average of 100 scans and resolution of 4 cm^{-1} at 773 K. The spectrum of the sample after the whole pretreatment (He degassing) was used as background. Two different procedures were used: dynamic (flowing gas—30 ml/min) and static (closed chamber) measurements.

Programmed thermodesorption of propane (TPD-C_3H_8) was done to verify the stability of surface species occurring during desorption of Pd/Al_2O_3 and $Pd/CeO_2/Al_2O_3$ catalysts. These experiments were performed with the adsorption of 1% C_3H_8/He flow at 773 K for 30 min at 50 ml/min and then after purge desorbed passing a He flow or a mixture of 5%O_2/He at 50 ml/min, rising the temperature at 10 K/min up to 773 K. The exit gases were analyzed by a quadrupole mass spectrometer (Balzers Prisma-QMS 200).

3. Results and discussion

3.1. Diffuse reflectance spectra (DRS) UV–vis

The diffuse reflectance spectra of Pd/Al_2O_3 and $Pd/CeO_2/Al_2O_3$ catalysts are presented in Fig. 1, prior to and following reaction. The Schuster–Kubelka–Munk (SKM) equation $F(R) = (1 - R)^2/2R$ was used along the ordinate instead of apparent absorbance, where R is the reflectance. All spectra presented $F(R)$ values less than 1, indicating absence of mirror reflectance on the sample. As γ-Al_2O_3 was used as reference it is possible to evaluate the oxidation state of Pd and Ce. Samples aged in the reaction system were analyzed without pretreatment.

The spectra of the fresh Pd/Al_2O_3 catalyst (a) presents the band centered at 400 nm, which represents PdO and is attributed to the transition band d–d of palladium [21]. It also presents a shoulder at 290 nm due to the charge transfer metal–ligand [22]. Aged samples (c) and (d) display similar bands in addition to another band at

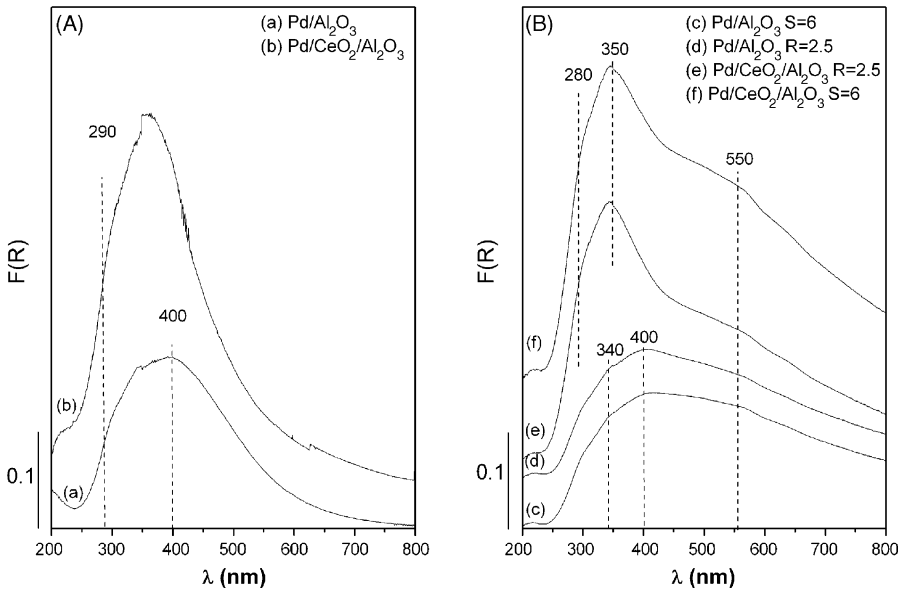

Fig. 1. Diffuse reflectance spectra (UV–vis) of Pd/Al_2O_3 and $Pd/CeO_2/Al_2O_3$ fresh (A) and after different reaction cycles for 48 h (B).

340 nm, which is attributed to the presence of Pd–OH species [23], while the band around 550 nm suggests the formation of a transition d–d band of palladium [24].

The enlargement of the adsorption band of the aged Pd/Al_2O_3 samples indicate the presence of metallic Pd^0 coexisting with PdO, as evidenced in the band 400 nm. As the wavelength used in this system (200–800 nm) is larger than the particle size (<100 nm), only the mean state value is calculated in the crystallite [25].

The wavelength relative to the semiconductor ceria can be evaluated to identify the presence of nanocrystallites, which cannot be detected by XRD. According to Bensalem et al. [26], ceria consists of crystallites of ≥20 nm mean size, displaying a sharp band appearing at $\lambda = 400$ nm. It was observed that the band at $\lambda \leq 375$ nm indicate small crystallites of ceria of the order of 8.5–4.5 nm. Fig. 1(e) and (f) shows characteristic bands of CeO_2 at 350 nm, ($Ce^{4+} \leftarrow O^{2-}$), which evidence the presence of nanoparticles of ceria. Additionally, a shoulder at 280 nm is attributed to the charge transfer of $Ce^{4+} \rightarrow O^{2-}$ [27,28], probably overlapping transition bands d–d of palladium. Moreover, the $Pd/CeO_2/Al_2O_3$ spectra (Fig. 1(e) and (f)), show intense bands centered at 550 nm that are assigned as reduced CeO_2 on the surface ($Ce^{3+} \rightarrow Ce^{4+}$) [29]. It is because for $S = 6$ (absence of oxygen) and for reducing condition ($R = 2.5$) this band evidences the presence of superficial Ce^{3+}.

3.2. X-ray diffraction (XRD)

Fig. 2 shows the XRD patterns of Pd/Al_2O_3 catalysts after pretreatment steps and time on stream under flowing gas mixture ($R = 2.5$) at 773 K. Characteristic diffraction lines of γ-Al_2O_3 with a cubic unit cell and space group Fd3m (PDF: 10-0425; $a = b = c = 0.79$ nm) were detected in all diffractograms with diffraction peaks at $2\theta = 37.8^\circ$ ($\langle 3\,1\,1\rangle$, $I = 80\%$), 46° ($\langle 4\,0\,0\rangle$, $I = 100\%$) and 66.5° ($\langle 4\,0\,0\rangle$, $I = 100\%$). Additionally, in fresh samples, were detected characteristic diffraction peaks of gibbsite (γ-$Al(OH)_3$) at $2\theta = 18.2^\circ$ ($\langle 0\,0\,2\rangle$, $I = 100\%$) and $2\theta = 20^\circ$ ($\langle 1\,1\,0\rangle$, $I = 70\%$), which has a monoclinic unit cell with space group P21/n (PDF: 33-0018; $a = 0.86$, $b = 0.5$ and $c = 0.97$ nm).

The transformation between alumina phases strongly depends on the precursors and the thermal treatment used in their stabilization [30]. According to Hill et al. [31], the gibbsite transition follows the trend: 373 K (gibbsite) → 473 K (gibbsite + boehmite) → 573 K (boehmite + χ-Al_2O_3) → 673 K (boehmite + χ-Al_2O_3) → 773 K (γ-Al_2O_3) → 873–1073 K (γ-Al_2O_3) → 1173–1373 K (γ-, δ- and θ-Al_2O_3) → 1473 K (α-Al_2O_3). In short, the thermal dehydration of gibbsite yields bohemite, which by additional annealing is transformed into γ-Al_2O_3. Under higher temperatures, it dehydrates to form corundum (α-Al_2O_3).

After He degassing (Fig. 2(b)), the gibbsite diffraction peaks disappeared and the intensity of γ-Al_2O_3 peaks increased in comparison to the fresh one (Fig. 2(a)), suggesting a gibbsite transition to γ-Al_2O_3. Concurrently, characteristic diffraction line of metallic Pd at $2\theta = 39.8^\circ$ (PDF: 46-1043; $a = b = c = 0.389$ nm) attributed to $\langle 1\,1\,1\rangle$ plane was detected, suggesting PdO reduction (PDF: 41-1107; $a = 0.3046$, $b = 0.3046$ and $c = 0.539$ nm) even under He flow at 773 K. The exposure to reaction mixture (Fig. 2(d)–(g)) shows palladium in metallic state. The broadening of palladium diffraction lines suggests the existence of small particles even after reaction during 20 h.

Fig. 3 shows the X-ray diffractograms of the $Pd/CeO_2/Al_2O_3$ catalyst under several treatments. Characteristic diffraction lines

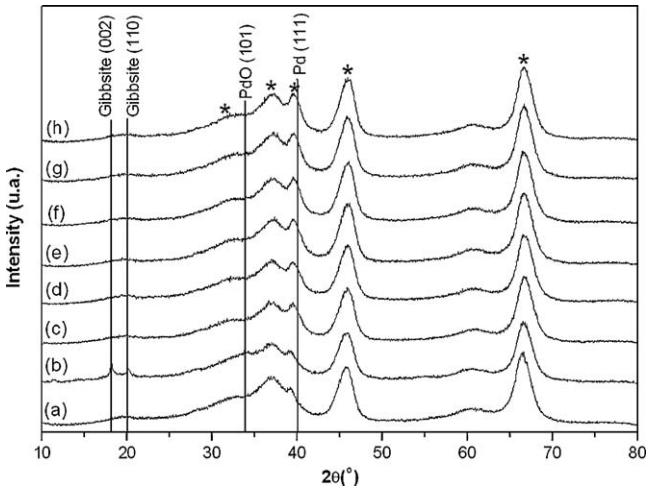

Fig. 2. XRD patterns of fresh γ-Al_2O_3 (a) and Pd/Al_2O_3 catalyst: fresh (b), after He degassing (c), reduction with H_2 (d), He degassing and reaction ($R = 2.5$; 773 K) for 1 h (e), 3 h (f), 8 h (g) and 20 h (h). Characteristic diffraction lines of γ-Al_2O_3 are indicated by (*).

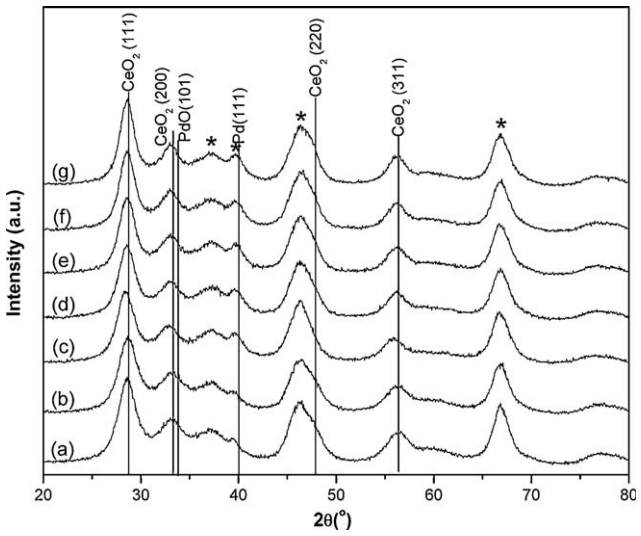

Fig. 3. XRD patterns of $Pd/CeO_2/Al_2O_3$ catalyst fresh (a), after oxidation in $5\%O_2$/He followed by He degassing (b), reduction with H_2 (c), He degassing and reaction ($R = 2.5$; 773 K) for 1 h (d), 3 h (e), 8 h (f) and 20 h (g). Characteristic diffraction lines of γ-Al_2O_3 are indicated by (*).

of CeO_2 at $2\theta = 28.5^\circ$ ($\langle 1\,1\,1\rangle$, $I = 100\%$), 33.2° ($\langle 2\,0\,0\rangle$, $I = 30\%$), 47.5° ($\langle 2\,2\,0\rangle$, $I = 52\%$) and 56.3° ($\langle 3\,1\,1\rangle$, $I = 42\%$) with fluorite structure and space group Fm3m (PDF: 34-0394; $a = b = c = 0.5411$ nm) were detected together with γ-Al_2O_3, PdO and Pd diffraction lines, also detected in Pd/Al_2O_3 catalyst.

An ideal CeO_2 crystal has a cubic, fluorite-type structure with space group Fm3m, where the cerium atom is at the center of a body central cube with eight oxygen atoms situated at the corners. Each cerium ion is cubic eight coordinated to oxygen ions and each oxygen is tetrahedrally coordinated to four cerium ions. There are four molecules per unit cell of CeO_2 crystal [32].

A possible interaction between alumina and ceria in the $Pd/CeO_2/Al_2O_3$ catalyst was not detected in the diffraction pattern. The high amorphous character of the samples can be deduced from the high level of noise detected in the patterns. Besides, there is no evidence of CeO_2 (Ce^{4+}) bulk reduction, even in reducing atmosphere (Fig. 3(c)). After reduction, the CeO_2 peak diffraction ($\langle 1\,1\,1\rangle$ plane) was shifted to lower 2θ values (-0.2°) and stable after 20 h on stream (-0.11°), as seen in Fig. 3(g). According to Sadi et al. [33], the shift of the peaks can be ascribed to the presence of CeO_{2-x} species and oxygen vacancies in the ceria network. Several authors [34–36] claim that bulk reduction of CeO_2 and Ce_2O_3 occurs only after 1200 K besides formation of $CeAlO_3$ and $CeO_{1.83}$ near to 1100 K. Despite that, the formation of ceria reduced species on surface cannot be ruled out. Through TPR measurements, Feio et al. [34] showed the formation of nonstoichiometric cerium oxides (CeO_{2-x}) at approximately 633 K. Besides, the metal deposition on ceria surface causes easier reduction of CeO_2 surface [14]. In consequence of these results, although the bulk phase is mainly formed of CeO_2 (Ce^{4+}), it can be discarding the reduction of ceria surface, which is in accordance with DRS measurements.

Palladium diffraction lines on CeO_2 supported catalyst ($Pd/CeO_2/Al_2O_3$) are broader than on Pd/Al_2O_3 catalyst, suggesting better dispersion and smaller crystallite sizes. Particularly for the $Pd/CeO_2/Al_2O_3$ catalyst, the diffraction lines of γ-Al_2O_3, CeO_2, PdO and metallic Pd are overlapping in diffractograms, making it difficult to discern palladium lines.

Detecting and measuring the nanoparticle size of active phases in metal supported catalysts is very important for a full characterization of the complex nanostructure of these composite materials, which is strictly connected to their catalytic behavior [37]. Some of the vacancy properties in nanocrystalline materials can be inferred by refining the crystalline structure of the phases in the sample. This is done by modeling the crystalline structure and size effects; the model is used for simulating the X-ray of the neutron diffraction pattern produced by the sample. The parameters involved in the model are varied until the theoretical diffraction pattern fits as well as possible to the experimental results [32]. The Rietveld technique is used to refine crystalline structures from a polycrystalline model. The Rietveld refinement provides not only information about concentration phases and crystallite sizes in the samples but information regarding to unit cell parameter and vacancies in the network. Fresh γ-Al_2O_3 or after degassing in He at 773 K (for treated and aged samples) were used as background for the refinement.

The good correspondence between experimental data and simulated curve was represented by a slight difference between the profiles (curve $Y_{obs} - Y_{cal}$). The refinement was applied in all pretreatment steps (after reduction shown in Fig. 4) and after reaction (1, 3, 8 and 20 h). A good correlation was obtained in all conditions. Therefore, the refinement provides a complete differentiation between the phases in the samples (Fig. 5). After deconvolution, the mean crystallite sizes were calculated for CeO_2, Pd^0 and PdO at the higher intensity planes: $\langle 1\,1\,1\rangle$, $\langle 1\,1\,1\rangle$ and $\langle 1\,0\,1\rangle$, respectively. Table 1 displays the results of crystallite sizes under several treatments and after reaction ($R = 2.5$) during 1, 3, 8 and 20 h. The lattice cell parameter from CeO_2 is also reported. The crystallite size and lattice cell parameter were determined by means of the Rietveld refinement.

According to Table 1, the sintering of Pd particles was not detected, even after 20 h of reaction. The presence of crystalline CeO_2 in $Pd/CeO_2/Al_2O_3$ catalyst favors the formation of dispersed Pd-metal particles ($d \sim 3.5$ nm) as compared to the Pd/Al_2O_3 catalyst, which contain larger Pd-metal particles ($d \sim 6$ nm), suggesting

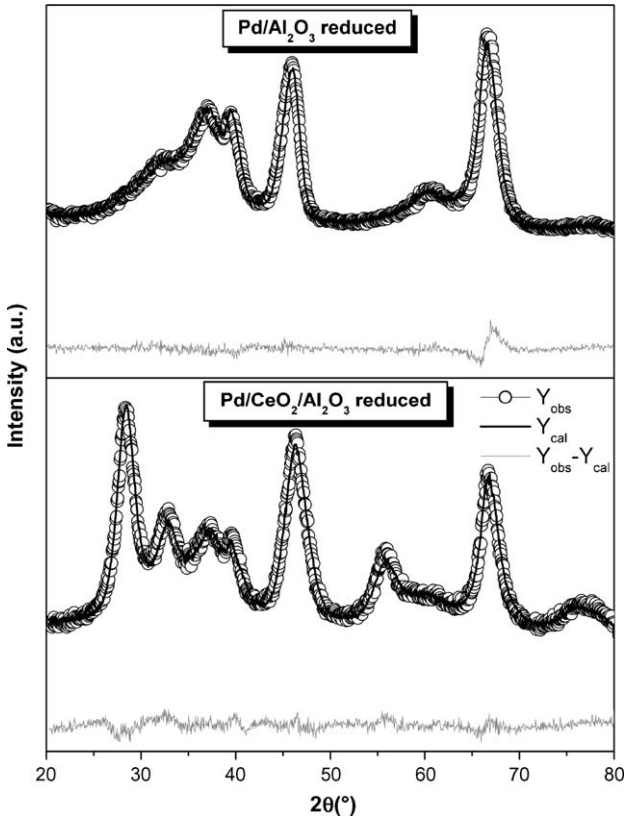

Fig. 4. Rietveld refinement of catalysts after reduction in H_2 at 773 K. Experimental data are indicated by circles and the continuous line is the calculated curve after refinement. The lower curve represents the difference between the experimental data and the calculated curve.

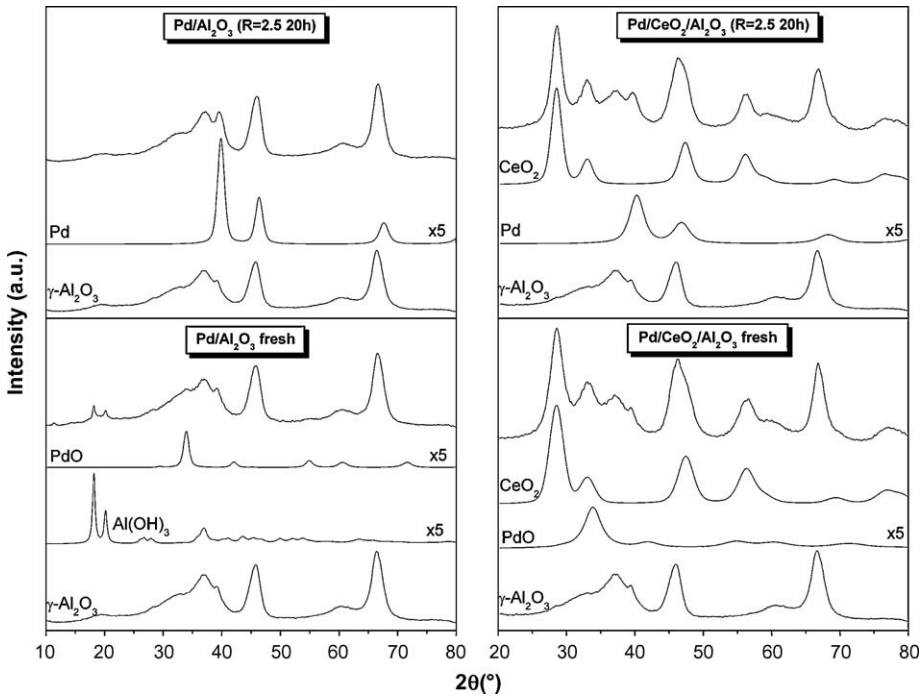

Fig. 5. Phase deconvolution through Rietveld refinement.

strong interaction between palladium–ceria. The cerium content is responsible for PdO stabilization because this phase remains after He degassing, which did not occur in the Pd/Al_2O_3 catalyst. Besides, the $Pd/CeO_2/Al_2O_3$ catalyst presents smaller PdO crystallite size ($d \sim 3$ nm) as compared to Pd/Al_2O_3 ($d \sim 8$ nm).

However, to explain the contradiction of chemisorption and *in situ* XRD results it is noteworthy to mention that we observed through CO infrared measurements [16] significant changes in the CO spectra for the PdCe-acac catalyst. Besides linear and bridged CO bands two new bands were observed which were attributed to cationic species of palladium. The existence of electron-deficient Pd species in the presence of ceria was also observed by Shyu et al [38] and Sass et al [39]. However, the presence of Pd^{2+} suggests incomplete reduction of PdO. Thus, the correct dispersion obtained by H_2 chemisorption increases, because the total metallic atoms decrease, and hence the crystallites decrease, in accordance with the *in situ* XRD measurements.

The interaction with ceria favors the redispersion of Pd crystallites in a structure with predominance of Pd(1 1 1) orientation, according to Badri et al. [40]. Moreover, previously [24] we showed through XPS after reaction and under similar conditions that the Pd/Al ratio changed markedly from 0.0018 for Pd/Al_2O_3 to 0.11 for the Pd/CeO_2 $/Al_2O_3$, suggesting higher dispersion or the presence of smaller particles, as confirmed here by XRD results.

The refinement of CeO_2 crystalline showed that lattice cell parameter increased as compared to a perfect cubic structure (PDF: 34-0394; $a = 0.5411$ nm) after reaction and under reaction conditions, indicating an expansion of the lattice cell volume. The lattice defects on ceria network could be indicative of oxygen deficient species (CeO_{2-x}) formation. Another evidence for this probable

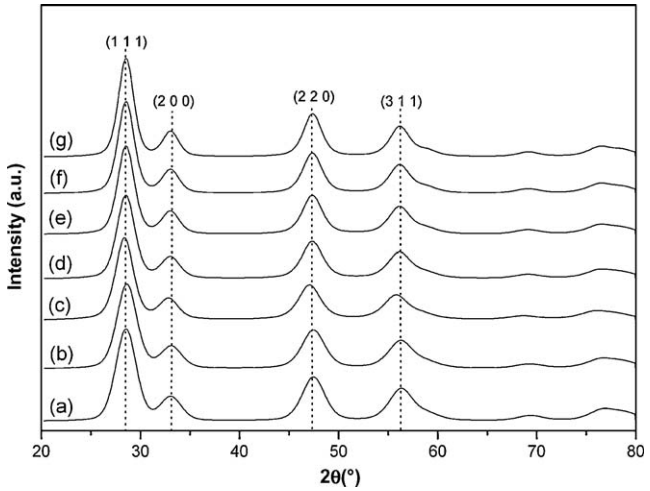

Fig. 6. Rietveld refinement plot of $Pd/CeO_2/Al_2O_3$ catalyst (CeO_2 planes) fresh (a), after oxidation in 5%O_2/He followed by He degassing (b), reduction with H_2 (c), He degassing and reaction ($R = 2.5$; 773 K) for 1 h (d), 3 h (e), 8 h (f) and 20 h (g).

Table 1
Average crystallite sizes and CeO_2 lattice cell parameter.

Treatment	Pd/Al_2O_3		$Pd/CeO_2/Al_2O_3$			
	D_{Pd} (nm)	D_{PdO} (nm)	Lattice parameter (nm)	D_{CeO_2} (nm)	D_{Pd} (nm)	D_{PdO} (nm)
Fresh	–	8.1	0.5421	3.4	–	2.8
He	6.3	–	0.5401	3.5	–	2.0
Reduction	5.9	–	0.5480	3.8	3.4	–
$R = 2.5$, 1 h	5.7	–	0.5444	3.9	3.4	–
$R = 2.5$, 3 h	5.8	–	0.5447	4.1	3.4	–
$R = 2.5$, 8 h	5.8	–	0.5446	4.3	3.5	–
$R = 2.5$, 20 h	6.1	–	0.5442	4.5	3.4	–

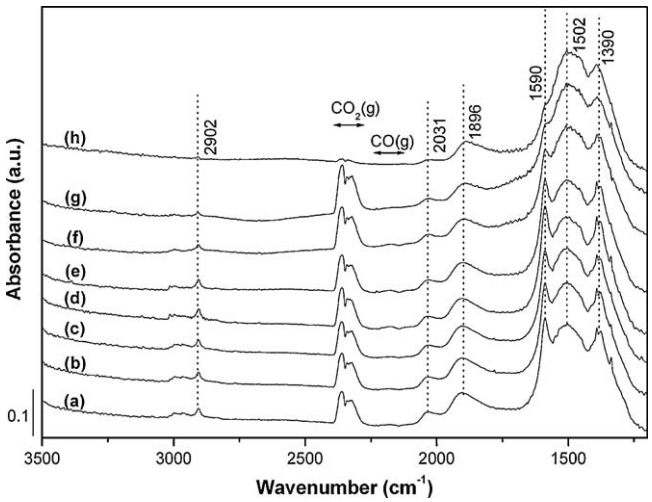

Fig. 7. DRIFT spectra for $Pd/CeO_2/Al_2O_3$ catalyst at 773 K under O_2/C_3H_8 ($R = 2.5$) flow during 5′ (a), 15′ (b) and 20′ (c). Chamber was closed during 1′ (d), 5′ (e), 15′ (f) and 20′ (g) under O_2/C_3H_8 atmosphere. At last, He degassing at 773 K during 10′ (h).

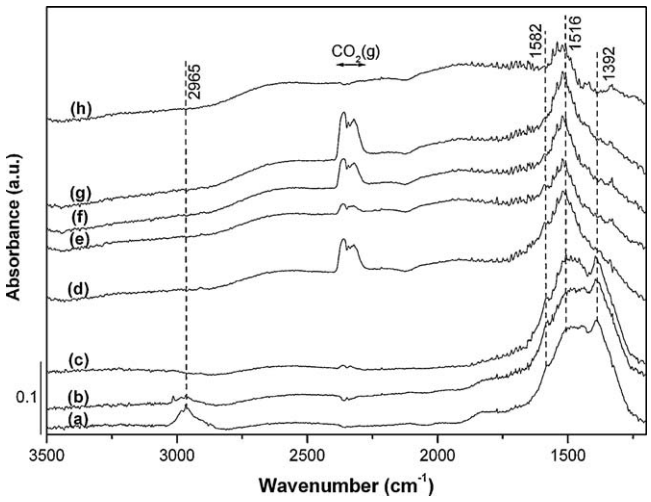

Fig. 8. DRIFT spectra for $Pd/CeO_2/Al_2O_3$ catalyst at 773 K. Adsorption under $1\%C_3H_8$/He during 10′ (a) and closed chamber for 5′ (b) under $1\%C_3H_8$/He atmosphere. He degassing during 10′ (c). Adsorption under $5\%O_2$/He during 1′ (d) and 5′ (e). Chamber was closed during 2′ (f) and 5′ (g) under O_2/C_3H_8. At last, He degassing at 773 K during 10′ (h).

CeO_{2-x} formation, as discussed earlier, is the negative shift of CeO_2 ⟨1 1 1⟩ peak. These results are supported by a remarkable increase of cell parameter under reducing conditions (0.5480 nm) in comparison to the fresh catalyst (0.5421 nm). Under reaction conditions, the values of cell parameter situated between these extremes due to simultaneous presence of reductive and oxidative compounds in gas phase. The changes in lattice cell parameter suggest high oxygen mobility inside the fluoritic structure, facilitating formation of CeO_{2-x} species. Additionally, the increase in CeO_2 crystallite size (Table 1) and diffraction peaks sharpening (Fig. 6) suggest a slight sintering of these particles.

3.3. Diffuse reflectance infrared fourier transform spectroscopy (DRIFTS)

Fig. 7 shows a set of *in situ* DRIFTS spectra for the $Pd/CeO_2/Al_2O_3$ catalyst under O_2/C_3H_8 ($R = 2.5$) flow. Bands located in the range of 2030–1900 cm^{-1} could be attributed to CO adsorbed on metallic palladium (Pd^0). According to Demoulin et al. [41], bands in the range 2100–1800 cm^{-1} reveal the presence of CO adsorbed on Pd^0, where linear CO on Pd^0 (Pd^0–CO) absorbs at 2100–2000 cm^{-1}, whereas bridging CO ($Pd_x{}^0$–CO) absorbs at 1900–1800 cm^{-1}. The absorption bands centered at 2031 and 1896 cm^{-1} (Fig. 7) could be ascribed to CO adsorbed in linear and bridge form, respectively.

The frequency of the CO adsorbed species increases with the oxidation state of palladium [42]. Small absorption bands near 2107 cm^{-1} could be ascribed to palladium in higher oxidation state [43].

The absorption bands at 2353 and 2143 cm^{-1} are characteristic for gaseous CO_2 and CO, respectively [44]. There is no evidence of CO adsorption on ceria sites, since bands located near to 2170 (CO–Ce^{4+}) and 2120 cm^{-1} (CO–Ce^{3+}) were not observed. The bands in the range of 2240–2200 cm^{-1} are usually attributed to CO adsorbed on coordinative unsaturated Al^{3+} ions. Bands near 2200 cm^{-1} are assigned to CO adsorbed on coordinative unsaturated Al^{3+} ions in octahedral coordination while bands located around 2240 cm^{-1} are attributed to CO adsorbed on coordinative unsaturated Al^{3+} ions in tetrahedral coordination [45]. Under experimental conditions used in this work, these bands were not observed.

The bands raised at 1380 (ν_s OCO), 1390 (δ C–H) and 1590 cm^{-1} (ν_{as} COO) can be attributed to formate species, while bands around 2970 cm^{-1} are usually attributed to gaseous propane [46,47]. The band at 2902 cm^{-1} (δ C–H) is characteristic of the stretching vibrations of C–H bond, probably CH_2 (ads) and CH_3 (ads) species. According to the literature [10], monodentate carbonates exhibit bands at 1530–1470 cm^{-1} (ν_{as} COO^-), 1370–1300 cm^{-1} (ν_s COO^-) and 1080–1040 cm^{-1} (ν C–O), while bidentate carbonates present bands at 1620–1530 cm^{-1} (ν C–O), 1270–1250 cm^{-1} (ν_{as} COO) and 1030–1020 cm^{-1} (ν_s COO). Therefore, one can attribute bands located at 1550–1420 cm^{-1} (Fig. 6) to monodentate carbonates but we do not discard the overlapping with another surface species in the same region due to the narrow absorption range between them, as reported by Appel et al. [19] and Demoulin et al. [41]. Pretreatment eliminated CO_2 adsorbed from environment, i.e., the sample was absent of any surface species before the introduction of O_2/C_3H_8 flow. Hydroxyls may be formed during the propane + oxygen reaction, however, changes in the spectra were not sensible due to the darkness of the sample.

The adsorption of O_2/C_3H_8 ($R = 2.5$) under flow during 20 min (Fig. 7(a)–(c)) did not affect the overall absorption spectra. After closing chamber and evacuation (Fig. 7(e)–(g)), the formate band tends to decrease and at the same time gaseous CO_2 is released, suggesting decomposition of formate into CO_2, which indicates that formate is probably an intermediate in the oxidative steam reforming. The surface degassing at He flow (Fig. 7(h)) did not remove the surface species (formates/carbonates) showing that, under experimental conditions used in this work, these species are stable even under He flow at 773 K. Appel et al. [19], through TPD and FTIR measurements, claim that CO_2 adsorption at room temperature resulted in the formation of stable carbonate species on ceria surface even at 673 K.

Fig. 8 displays the *in situ* DRIFTS spectra for the $Pd/CeO_2/Al_2O_3$ catalyst. The objective of this step was to investigate the interaction of propane with the surface and subsequently the interaction of surface species created by propane adsorption with oxygen flow. The adsorption of 1% C_3H_8/He (Fig. 8(a)) results in the formation of carbonates and formates at the surface and present a characteristic absorption band of C_3H_8 gas (~2965 cm^{-1}). It suggests that propane chemisorbs at the interface metal-support, transforming in hydrocarbon fragment species (~2902 cm^{-1}), which react with alumina surface hydroxyls or oxygen structural of ceria generating $HCOO^-$ (formate) and m-$CO_3{}^{2-}$ (monodentate carbonate) intermediates. Fig. 8(c) shows again the stability of these species under He flow after 10 min at 773 K. Under these experimental conditions, propene formation was not detected in any technique adopted (DRIFTS, mass spectrometry and chroma-

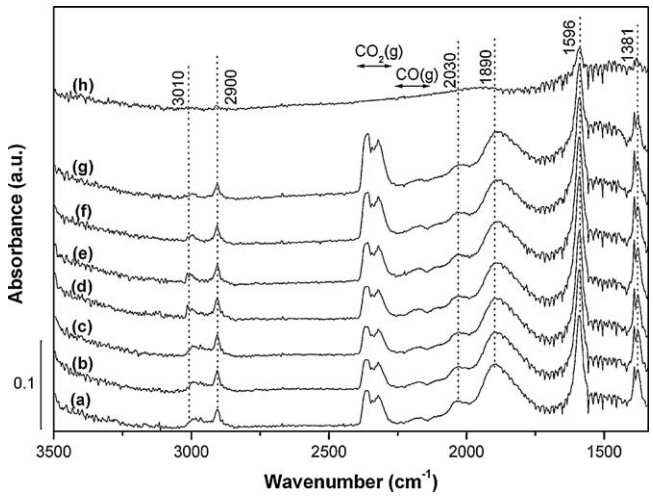

Fig. 9. DRIFT spectra for Pd/ Al_2O_3 catalyst at 773 K under O_2/C_3H_8 (R = 2.5) flow during 5′ (a), 15′ (b) and 20′ (c). Chamber was closed during 1′ (d), 5′ (e), 15′ (f) and 20′ (g) under O_2/C_3H_8 atmosphere. At last, He degassing at 773 K during 10′ (h).

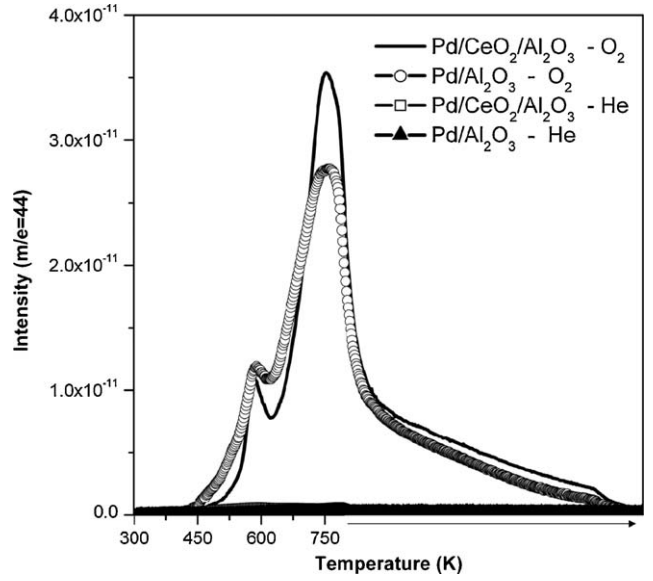

Fig. 10. CO_2 desorption (m/e = 44) for $Pd/CeO_2/Al_2O_3$ and Pd/Al_2O_3 under He or 5%O_2/He flow during TPD experiments.

tography), discarding the occurrence of ODH reaction (oxidative dehydrogenation), as reported by other authors [48,49]. After passing 5%O_2/He flow (Fig. 8(d)–(g)) the formate was consumed releasing CO_2. The intensity of carbonate decreased but remains on surface even after He degassing at 773 K for 10 min (Fig. 8(h)), suggesting that carbonates are not spectator species, but less reactive than formate and therefore, can be considered as a real intermediate species.

Fig. 9 displays the *in situ* DRIFTS spectra of the Pd/Al_2O_3 under O_2/C_3H_8 (R = 2.5) flow collected at 773 K. Also in this case, pretreatment eliminated surface species originally in the sample before introduction of reactant gas. The Pd/Al_2O_3 exhibits characteristic bands of gases CO_2 (~2353 cm^{-1}), CO (~2143 cm^{-1}) and of CO adsorbed on Pd° (linear ~2030 cm^{-1}; bridge ~1890 cm^{-1}), as well as gaseous C_3H_8 (~2970 cm^{-1}), formate (1380, 1390 and 1596 cm^{-1}) and the CH_z species (~2902 cm^{-1}). The main difference with the $Pd/CeO_2/Al_2O_3$ catalyst is the absence of carbonate bands (~1500 cm^{-1}). Therefore, the formate appearance suggests the propane adsorption at Pd/Al_2O_3 interface, while carbonate bands are located on ceria. Solymosi et al. [50] calculated the concentration of surface formate formed in the coadsorption of H_2 + CO_2 on Pd/Al_2O_3 catalyst through correlation between the integrated area of the formate absorption band (1600–1580 cm^{-1}) and the amount of surface formate groups greatly exceeds the number of surface Pd atoms (by an factor of 15), supporting the idea that the formation mainly resides on the support (γ-Al_2O_3). However, the coadsorption on raw alumina did not produce formate bands. Demoulin et al. [41] noticed that the stability of formates on oxide support is weaker than with palladium supported catalysts, indicating that, during the reaction, these species can migrate towards palladium and decompose or react.

3.4. Thermodesorption of propane (TPD-C_3H_8)

Programmed thermodesorption was done to verify the stability of surface species occurring during desorption of Pd/Al_2O_3 and $Pd/CeO_2/Al_2O_3$ catalysts. These experiments were performed with the adsorption of 1% C_3H_8/He flow at 773 K for 30 min at 50 ml/min and then after purge desorbed passing a He flow or a mixture of 5%O_2/He at 50 ml/min rising the temperature at 10 K/min up to 773 K.

Fig. 10 displays the CO_2 formation either with He and O_2 flow. Only CO_2 and water were observed when 5% O_2/He flow passed, which suggests that species such as formate and/or carbonate are stable under He flow. Propane was not detected indicating that it was transformed in formate or carbonate species after oxidation. Propene was not observed, that means, no oxidative dehydrogenation occurs, contrary to the literature [47,48]. Supporting the TPSR [17] and DRIFTS results, no H_2 and CO were detected in this temperature range under applied experimental conditions ($O_2/C_3H_8 > 5$).

The Pd/Al_2O_3 catalyst presented two desorption peaks of CO_2 at 575 and 740 K, which is evidence for existing formate at the surface of the Pd/Al_2O_3 catalyst with different degree of absorption on Pd particles. The $Pd/CeO_2/Al_2O_3$ shows more CO_2 formation than the Pd/Al_2O_3 catalyst, and suggests that this decomposition is due to formate and carbonate at higher temperature.

According to these results, we can propose the overall reaction pathway of propane autothermal reforming on $Pd/CeO_2/Al_2O_3$ catalysts:

Step 1—Hydrocarbon cracking

$$C_3H_8\,(g) \rightarrow C_3H_x\,(ads) + xH\,(ads) \rightarrow 3CH_z\,(ads) \quad (metal)$$

Step 2—Reaction between CH_z fragments and oxygen from support

$$CH_z\,(ads) + 2OH^- \rightarrow HCOO^-\,(ads) + (z+1)H\,(ads) \quad (alumina)$$

$$CH_z\,(ads) + CeO_2 \rightarrow m\text{-}CO_3{}^{2-}\,(ads) + CeO_{2-x} + yH\,(ads) \quad (ceria)$$

Step 3—Carbonate and formate decomposition under oxidative environment

$$2HCOO^-\,(ads) + 1/2O_2\,(g) \rightarrow 2CO_2\,(g) + H_2O(g) \quad (alumina)$$

$$m\text{-}CO_3{}^{2-}\,(ads) + CeO_{2-x} + O_2\,(g) + yH\,(ads) \rightarrow CeO_2 + CO_2\,(g) + H_2O\,(g) \quad (ceria)$$

Step 4—Carbonate and formate decomposition in absence of oxygen

$$HCOO^-\,(ads) \rightarrow CO_x\,(g) + H_2\,(g) \quad (alumina)$$

$$m\text{-}CO_3{}^{2-}\,(ads) + CeO_{2-x} + H_2O\,(g) \rightarrow CO_x\,(g) + H_2\,(g) + CeO_2 \quad (ceria)$$

Step 5—Water gas shift

$$xCO(ads) + CeO_2 \rightarrow CeO_{2-x} + xCO_2\,(g) \quad (ceria)$$

$$CeO_{2-x} + xH_2O\,(g) \rightarrow CeO_2 + xH_2\,(g) \quad (ceria)$$

The gas propane adsorbed on the metal-support interface may crack into hydrocarbon fragments (CH_z), as evidenced by the absorption band located around 2900 cm^{-1} (δ C–H). The adsorption

of C_3H_8 (Fig. 8) allows the formation of carbonates/formates on the surface even in the absence of oxygen in the feed. This means, the support supplies the oxygen either through alumina hydroxyls or structural oxygen from ceria (step 2). As discussed earlier, formates are mainly present on γ-Al_2O_3, while carbonates are located on ceria surface. The reaction between CH_z fragments and ceria surface (Ce^{4+}) generate carbonates and causes ceria surface reduction forming CeO_{2-x} species (step 3), supported by XRD measurements that showed the formation of deficient oxygen species (CeO_{2-x}) through an increase on ceria lattice cell parameter. Additionally, DRS measurements presented absorption band around 550 nm, attributed to reduced surface CeO_2 sites at the surface ($Ce^{4+} \rightarrow Ce^{3+}$ transfer charge) [28].

According to TPSR measurements [17], the oxygen excess in the feed ($R > 5$) resulted in total oxidation of propane releasing CO_2 and H_2O, without CO and H_2 formation. Under substoichiometric conditions ($R < 5$), the steam reforming occurs only after complete consumption of oxygen. Fig. 8 supports these results evidenced by CO_2 releasing without CO formation after 5% O_2/He flow. Therefore, the oxidation of formate/carbonate generates CO_2 and H_2O, restoring the surface ceria to the original state Ce^{4+} (step 3). This was confirmed by TPD of propane in the presence of oxygen. After complete oxygen consumption, the surface species (formate/carbonate) decomposes releasing steam reforming products (step 4). Water formed during oxidation is also responsible for restoring surface alumina hydroxyls (OH^-), which is essential to the formation of formate species (step 2). Additionally, carbonates are decomposed on ceria surface generating steam reforming products and restoring the oxygen from ceria. Besides, as verified and reported previously [17], ceria is active for the WGS reaction between CO adsorbed and water generated by oxidation, according to mechanism reported by Bunluesin et al. [51], as described in step 5.

4. Conclusions

XRD and DRS measurements indicate the presence of crystalline CeO_2 in Pd/CeO_2/Al_2O_3 that favors the formation of dispersed Pd-metal particles as compared to the Pd/Al_2O_3 catalyst, which contain large Pd-metal particles, suggesting strong interaction between palladium–ceria. Therefore, one can conclude that CeO_2 enhances and maintains the dispersion of Pd on bulk catalyst and prevents Pd from severe aggregation along the reaction because no sintering was detected even after 20 h of reaction. The changes in lattice cell parameter determined by Rietveld refinement suggested high oxygen mobility inside the fluoritic structure, facilitating formation of CeO_{2-x} species. The refinement was applied with good correlation between experimental data and simulated curve.

The DRIFTS and TPD measurements showed that propane adsorbs on metal-support interface cracking into hydrocarbon fragments and reacting with alumina hydroxyls and/or structured oxygen from ceria, generating $HCOO^-$ (formate) and/or m-CO_3^{2-} (carbonate). CO_x compounds are released after combustion of these carboxylate species (formate/carbonate) under oxidative environment. After complete consumption of oxygen in reaction mixture, the surface species decomposes releasing steam reforming products. The Pd/CeO_2/Al_2O_3 catalyst facilitates the formation of formate and carbonate species, whereas on Pd/Al_2O_3 catalyst prevail the formation of formate species, suggesting different reaction mechanisms.

Acknowledgements

The authors would like to acknowledge CNPq, Finep (Pronex) for the financial support. One of the authors (Wagner Faria) would like to thank FAPERJ for the scholarship.

References

[1] K. Adamson, Energy Policy 32 (2004) 1231.
[2] A.K. Avci, I. Ölsan, D.L. Trimm, Top. Catal. 22 (2003) 359.
[3] K. Narusawa, M. Hayashida, Y. Kamiya, H. Roppongi, D. Kurashima, K. Wakabayashi, JSAE Rev. 24 (2003) 41.
[4] S. Ahmed, R. Kumar, M. Krumpett, Fuel Cells Bull. 2 (1999) 4.
[5] I. Aartun, T. Gjenvan, M. Venvik, O. Görke, P. Pfeifer, M. Fathi, A. Holmen, K. Schubert, Chem. Eng. J. 101 (2004) 93.
[6] L. Pino, A. Vita, F. Cipitì, M. Laganà, V. Recupero, Appl. Catal. A 306 (2006) 68.
[7] B. Silberova, H.J. Venvik, J.C. Walmsley, A. Holmen, Catal. Today 100 (2005) 457.
[8] N. Laosiripojana, S. Assabumrungrat, J. Power Sources 158 (2006) 1348.
[9] P. Corbo, F. Migliardini, Int. J. Hydrogen Energy 32 (2007) 55.
[10] M. Schmal, M.M.V.M. Souza, V.V. Alegre, M.A.P. Silva, D.V. César, C.A.C. Perez, Catal. Today 118 (2006) 392.
[11] C. Descorme, R. Taha, N.M. Moral, D. Duprez, Appl. Catal. A 223 (2002) 287.
[12] A. Piras, A. Trovarelli, G. Dolcetti, J. Phys. Chem. B 28 (2000) L77.
[13] S. Colussi, C. Leitenburg, G. Dolcetti, A. Trovarelli, J. Alloys Compd. 374 (2004) 387.
[14] S. Damyanova, J.M.C. Bueno, Appl. Catal. A 253 (2003) 135.
[15] S. Wang, G.Q. Lu, Appl. Catal. B 19 (1998) 267.
[16] R.S. Monteiro, L.C. Dieguez, M. Schmal, Catal. Today 65 (2001) 77.
[17] W.L.S. Faria, L.C. Dieguez, M. Schmal, Appl. Catal. B 85 (2008) 77.
[18] J.L. Duplan, H. Praliaud, Appl. Catal. 67 (1991) 325.
[19] L.G. Appel, J.G. Eon, M. Schmal, Catal. Lett. 56 (1998) 199.
[20] J.H. Zhang, Y.Q. Yang, J.M. Shen, J.A. Wang, J. Mol. Catal. A 237 (2005) 182.
[21] A.B. Gaspar, L.C. Dieguez, Appl. Catal. A 201 (2000) 241.
[22] A. Rakai, D. Tessier, F. Bozon-Verduraz, N. J. Chem. 16 (1992) 869.
[23] M. Schmal, M.A.S. Baldanza, M.A. Vannice, J. Catal 185 (1999) 138.
[24] A.L. Guimarães, L.C. Dieguez, M. Schmal, Ann. Braz. Acad. Sci. 76 (2004) 825.
[25] M. Lyubovsky, L. Pfefferle, Catal. Today 47 (1999) 29.
[26] A. Bensalem, J.C. Muller, F. Bozon-Verduraz, J. Chem. Soc. Faraday Trans. 88 (1992) 153.
[27] M.I. Zaki, G.A.M. Hussein, S.A.A. Mansour, H.M. Ismail, G.A.H. Mekhemer, Colloids Surf. A 127 (1997) 47.
[28] A. Martinez-Arías, M. Fernández-Garcia, L.N. Salamanca, R.X. Valenzuela, J.C. Conesa, J. Soria, J. Phys. Chem. B 104 (2000) 4038.
[29] B.G. Mishra, G.R. Rao, J. Mol. Catal. A 243 (2006) 204.
[30] J.A. Wang, X. Bokhimi, A. Morales, O. Novaro, T. López, R. Gómez, J. Phys. Chem. B 103 (1999) 299.
[31] M.R. Hill, T.J. Bastow, S. Celotto, A.J. Hill, Chem. Mater. 19 (2007) 2877.
[32] J.A. Wang, J.M. Dominguez, A. Montoya, S. Castillo, J. Navarrete, M. Moran-Pineda, J. Reyes-Gasga, X. Bokhimi, Chem. Mater. 14 (2002) 4676.
[33] F. Sadi, D. Duprez, F. Gérard, A. Miloudi, J. Catal. 213 (2003) 226.
[34] L.S.F. Feio, C.E. Hori, S. Damyanova, F.B. Noronha, W.H. Cassinelli, C.M.P. Marques, J.M.C. Bueno, Appl. Catal. A 316 (2007) 107.
[35] M. Hietikko, U. Lassi, K. Kallinen, A. Savinäki, M. Härkonen, J. Pursiainen, R.S. Laitinen, R.L. Keiski, Appl. Catal. A 277 (2004) 107.
[36] S. Damyanova, C.A. Perez, M. Schmal, J.M.C. Bueno, Appl. Catal. A 234 (2002) 271.
[37] G. Fagherazzi, P. Canton, P. Riello, F. Pinna, N. Pernicone, Catal. Lett. 64 (2000) 119.
[38] J.Z. Shyu, K. Otto, W.L.H. Watkins, G.W. Graham, R.K. Belitz, H.S. Gandhi, J. Catal. 114 (1988) 23.
[39] A.S. Sass, V.A. Shvets, G.A. Savel'eva, N.M. Popova, V.B. Kazanskii, Kinet. Catal. 27 (1986) 777.
[40] A. Badri, C. Binet, J.-C. Lavalley, J. Chem. Soc., Faraday Trans. 92 (1996) 1603.
[41] O. Demoulin, M. Navez, P. Ruiz, Appl. Catal. A 295 (2005) 59.
[42] A. Martínez-Arias, M. Fernández-Gárcia, A. Iglesias-Juez, A.B. Hungría, J.A. Anderson, J.C. Conesa, J. Soria, Appl. Catal. B 31 (2001) 51.
[43] R. Craciun, W. Daniell, H. Knözinger, Appl. Catal. A 230 (2002) 153.
[44] L.H. Little, Infrared of Adsorbed Species, Academic Press, New York, 1966.
[45] M. Skotak, Z. Karpínski, W. Juszczyk, J. Pielaszek, L. Kepinski, D.V. Kazachkin, V.I. Kovalchuk, J.L. d' Itri, J. Catal. 227 (2004) 11.
[46] V. Ermini, E. Finocchio, S. Sechi, G. Busca, S. Rossini, Appl. Catal. 190 (2000) 157.
[47] R.W. van den Brink, P. Mulden, R. Lown, G. Sinquin, C. Petit, J.P. Hindermann, J. Catal. 180 (1998) 153.
[48] D. Creaser, B. Anderson, Appl. Catal. A 141 (1996) 131.
[49] T. Maillet, C. Solleau, J. Barbier, D. Duprez, Appl. Catal. B 14 (1997) 85.
[50] F. Solymosi, A. Erdöhelyi, M. Lancz, J. Catal. 95 (1985) 567.
[51] T. Bunluesin, R.J. Gorte, G.W. Graham, Appl. Catal. B 15 (1998) 107.